Journal of Catalysis 260 (2008) 342–350

Contents lists available at ScienceDirect

Journal of Catalysis

www.elsevier.com/locate/jcat

The synthesis of highly dispersed noble and base metals on silica via strong electrostatic adsorption: II. Mesoporous silica SBA-15

L. Jiao, J.R. Regalbuto *

Department of Chemical Engineering, University of Illinois at Chicago, 810 S Clinton St, Chicago, IL 60607, USA

ARTICLE INFO

Article history:
Received 7 March 2008
Revised 31 August 2008
Accepted 19 September 2008
Available online 1 November 2008

Keywords:
Catalyst preparation
Synthesis
Strong electrostatic adsorption
Platinum
Palladium
Ruthenium
Copper
Cobalt
Ammine SBA-15
Point of zero charge
PZC

ABSTRACT

The catalyst synthesis method of strong electrostatic adsorption (SEA) was applied to mesoporous silica SBA-15. pH shift control experiments were performed to determine the point of zero charge (PZC) of SBA-15. Adsorption–pH surveys of various noble and base metal ammines (Pt, Pd, Cu, Co, Ru ammines) on SBA-15 were carried out to determine the pH of maximum uptake. Adsorption kinetics also were examined. SBA-15-supported Pt, Pd, and Co materials were prepared via SEA and dry impregnation (DI) methods for further characterization via TPR and STEM. The results suggest that the adsorption mechanism of all metal ammines is largely electrostatic, and that the adsorption can approach equilibrium in a very short time (within 5 minutes). Metal complexes deposit homogeneously on the internal surface area of SBA-15. Low-temperature-reducing metals, such as Pt and Pd, form very well-dispersed (1.3 to 2.0 nm) nanoparticles after reduction, with small standard deviation, at loadings on the order of 10 wt%. Cobalt particles were larger (7.3–9.2 nm), because the much higher temperature required for reduction of the adsorbed cobalt ammine complex led to metal sintering. The SEA-prepared Co particles were still much smaller than the DI-prepared particles, which could be reduced at much lower temperature.

1. Introduction

Since the discovery of silica with highly ordered mesoporous structure, such as M41s [1] and SBA-15 [2], many applications of these materials in areas of catalysis, separation, adsorption, and drug delivery have been proposed and developed [3–5]. The unique properties of these silica materials are their high surface areas, extremely narrow pore size distributions, adjustable pore sizes, and the presence of silanol groups. SBA-15 silica has thicker pore walls (3.1–6.4 nm) and larger pore sizes (in the range of 3.6–10.0 nm) compared with MCM-41 and MCM-48, which may facilitate the diffusion of relative bulky molecules and the mobility of nanostructured metals [6].

In the first part of this work [7], we presented the synthesis strategy of strong electrostatic adsorption (SEA) [8] for a series of highly dispersed metals of noble and base metals from ammine complexes over amorphous silica. The correlation between strong interaction during impregnation and small size of reduced metal particles was determined. In this part, we extend the investigation of SEA of metal ammine complexes to mesoporous silica SBA-15.

A literature survey of preparation methods for Pt/SBA-15, Pd/SBA-15, Cu/SBA-15, Co/SBA-15, and Ru/SBA-15 is summarized in Table 1. The table gives the metal loading, subsequent calcination and reduction temperatures, and metal dispersion or particle size for the different methods of metal addition. The hexachloride precursor appears to be the current precursor of choice for Pt synthesis over SBA-15 [9–15]. The single exception is a deposition–precipitation method with urea in which the tetraammine was used [12]; this method did not give as high dispersion as chloroplatinic acid with incipient wetness. With this precursor, small particles are obtained only at low loadings, such as 0.1–0.6 wt% [10]. For palladium, reasonably small particles are produced using chloride [16], acetate [17], and ammine [18] precursors, the latter by "ion impregnation" (which, as stated in Part I, we believe is better termed "electrostatic adsorption"). Low loadings appear to have been used in all cases. Incipient wetness with copper yielded large particles of 200–300 Å, whereas a "postgrafting" method brought this down to 50 Å [19]. Incipient wetness or wet impregnations have been used with cobalt nitrate [20–22], and in no case was a dispersion greater than about 20% reported for cobalt. Wet impregnations with ruthenium yielded 20–50 Å particles at low weight loadings [23], whereas an ultrasound-assisted polyol method could produce some small particles at high Ru loadings [24].

Several investigators have used electrostatic adsorption of the metals into MCM-41 [25–27] (also termed "ion exchange" [26] and

* Corresponding author.
E-mail address: jrr@uic.edu (J.R. Regalbuto).

0021-9517/$ – see front matter
doi:10.1016/j.jcat.2008.09.023

Table 1
Summary of the literature on the method of preparation for SBA-15-supported Pt, Pd, Cu, Co, and Ru catalysts.

Ref.	Metal loading (wt%)	Surface area (m^2/g)	Pd precursor	Method	Calcination temp. (K)	Reduction temp. (K)	Dispersion (%)	Particle size (Å)
[9]	15	353	H_2PtCl_6	IWI	–			104
[10]	0.1	782	H_2PtCl_6	IWI	–	623	100	
[10]	0.6	782	H_2PtCl_6	IWI	–	623	43.5	
[10]	1	782	H_2PtCl_6	IWI	–	623	29.4	
[11]	0.1	801	K_2PtCl_4	IWI	–	573		55
[12]	0.1	900	K_2PtCl_4	Sol–gel	773	673	8.0	
[12]	0.1	750	H_2PtCl_6	IWI	773	673	24.6	
[13]	0.5	~860	$[Pt(NH_3)_4](OH)_2$	DP	573		37	34
[13]	0.5	~860	H_2PtCl_6	IWI	573		44.5	25
[14]	~8	553	H_2PtCl_6	WI	–	373–573		20
[15]	0.73	765	H_2PtCl_6	Alcohol reduction	623	–		17
[15]	0.90	765	H_2PtCl_6	Alcohol reduction	723	–		26
[15]	0.95	765	H_2PtCl_6	Alcohol reduction	723	–		29
[15]	0.46	765	H_2PtCl_6	Alcohol reduction	723	–		36
[15]	1.0	765	H_2PtCl_6	Alcohol reduction	723	–		36
[16]	–	~800	$PdCl_2$	IWI	–	–		30–50
[17]	0.6	808	$Pd(NH_3)_4Cl_2$	IE	823	573	32	36
[18]	0.5	40	$Pd(CH_3COO)_2$	WI	723	–	66	17
[19]	–	815	$Cu(NO_3)_2$	Postgrafting	773	823		50
[19]	–	815	$Cu(NO_3)_2$	IWI	773	823		200–300
[20]	10	842	$Co(NO_3)_2^+$ ethanol	WI	573	673	20.5	
[20]	20	842	$Co(NO_3)_2^+$ ethanol	WI	573	673	11.2	
[20]	30	842	$Co(NO_3)_2^+$ ethanol	WI	573	673	9.3	
[20]	40	842	$Co(NO_3)_2^+$ ethanol	WI	573	673	7.3	
[21]	6.95	679	$Co(NO_3)_2$	IWI	773	–	13.9	
[21]	6.95	887	$Co(NO_3)_2$	IWI	773	–	10.6	
[22]	15	662	$Co(NO_3)_2$	IWI	773		11.7	80
[23]	1.0	750	$RuCl_3^+$ methanol	WI	–	423		20–50
[24]	14	550	$RuCl_3$	Ultrasound-assisted polyol method	Dried at R.T.			20–60, 100–200

IWI: incipient wetness impregnation or dry impregnation; WI: wet impregnation; IE: ion exchange.

"selective adsorption" [27]). Pt particles in the range of 1.1–2.1 nm have been synthesized at about 1 wt% by adsorption at pH 8 [25,26], whereas Ru particles of about 1.5 nm have been produced at 1.9 wt% by adsorption at pH 7.5 [27]. These syntheses were performed at a pH of 7.5–8 to minimize degradation of the MCM-41 structure through dissolution.

In the present work, we carried out adsorption surveys of a series of metal ammines (Pt, Pd, Cu, Co, Ru ammine complexes) at various pH values and further characterized Pt/SBA-15, Pd/SBA-15, and Co/SBA-15 materials synthesized at the optimal pH. We determined the appropriate reduction temperature by temperature-programmed reduction (TPR), particle size and distribution by scanning transmission electron microscopy (STEM), and metal distribution by energy-dispersive X-ray spectroscopy (EDXS). We compared the SEA preparations with materials prepared via the traditional dry impregnation method. We demonstrate that the simple, rational preparation method of SEA can be readily applied to mesoporous silica for synthesizing ultra-small metal particles even at very high metal loadings.

2. Experimental

2.1. Material preparation

SBA-15 was obtained from Professor de Jong's group at Utrecht University (designated SBA-15-1 and SBA-15-2) and from Dr. Jianfeng Yao at Monash University (designated SBA-15-3). The general procedure for synthesizing SBA-15 was as follows. First, 4.0 g of triblock copolymer Pluronic P123 was dissolved in 30 g of water and 120 g of 2 M HCl solution under stirring at 35 °C. Then 8.50 g of TEOS was added into the solution under continuous stirring at 35 °C for 20 h. The resulting mixture was aged at 80 °C overnight without stirring. The solid product was recovered, washed, and air-dried at room temperature. The yield was around 98% (based on silicon), which is comparable to that from the syntheses described above. Calcination was carried out by slowly increasing the temperature from room temperature to 500 °C over 8 h and heating at 500 °C for 6 h [28]. The textural properties of the SBA-15 samples, obtained with a Micromeritics 2020 ASAP surface area and pore size analyzer, are listed in Table 2.

Table 2
Textural properties of the SBA-15 and SEA-prepared Pt/SBA-15 material.

Sample	BET surface area (m^2/g)	Pore volume (cm^3/g)	Mean pore diameter (Å)
SBA-15-1	494	0.514	41.7
SBA-15-2	581 ± 7	0.566 ± 0.010	40.3 ± 0.7
SBA-15-2 (1 h, pH 10)	531	0.718	54.0
PTA/SBA-15-2 9.15% Pt, 1 h, pH 10, dried at R.T.	365	0.500	54.8
PTA/SBA-15-2 9.15% Pt, 1 h, pH 10, dried at 100 °C	391	0.528	54.0
Pt/SBA-15-2 9.15% Pt, 1 h, pH 10, reduced at 160 °C	493	0.672	54.5
SBA-15-3	998	0.936	37.5

2.2. pH shift and PZC measurements

The three mesoporous silicas SBA-15-1, SBA-15-2, and SBA-15-3 were weighed out to obtain surface loadings of 1000 and 10,000 m^2/L for 50 mL of solution. Solutions were made up at various pH values in the range of 1–13 using HNO_3 and NaOH. Then 50 mL of each solution was added to the silica in 60-mL polypropylene bottles. The solutions were shaken for 1 h. ICP was used to measure the amount of dissolved Si. Final pH measurements were obtained using a general combination pH electrode. At sufficiently high surface loadings, the plateau of the pH shift plot corresponds to the PZC of the support [29].

2.3. Adsorption surveys

SBA-15 was weighed to obtain a surface loading of 1000 m^2/L with 50-mL solutions into 60-mL bottles. Palladium(II) tetraammine chloride monohydrate ($Pd(NH_3)_4Cl_2$, 99.9%), copper(II) tetraammine sulfate ($Cu(NH_3)_4SO_4$, 98%), cobalt(III) hexaammine chloride ($Co(NH_3)_6Cl_3$, 99%), ruthenium(II) hexaammine chloride ($Ru(NH_3)_6Cl_2$, 99.9+%), ruthenium(III) hexaammine chloride ($Ru(NH_3)_6Cl_3$, 98%), and nickel(II) hexaammine chloride ($Ni(NH_3)_6Cl_2$, 99.999%) precursors were obtained from Aldrich. These are designated PdTA, CuTA, CoHA, Ru(II)HA, Ru(III)HA, and NiHA, respectively. Pd, Cu, Co, Ru and Pt ammine solutions were made up at 200 ppm. The initial pH values were adjusted in the range of 4–13 for the adsorption of $[Pd(NH_3)_4]^{+2}$, $[Co(NH_3)_6]^{+3}$, $[Ru(NH_3)_6]^{+3}$, and $[Ru(NH_3)_6]^{+2}$ over silica. For the purchased and self-prepared $[Cu(NH_3)_4]^{+2}$ complexes, the adsorption surveys were performed at the initial pH values of 10–13, because the copper ammine complex is not stable in the acidic pH range. The initial pH values were measured, and 50 mL of solution was added to the SBA-15 and shaken for 1 and 24 h. Final pH values were measured, and 5-10 mL of solution was filtered for ICP analysis of the adsorbate metals as well as dissolved Si. The metal surface density, Γ_{metal}, was calculated at the concentration of metal adsorbed divided by the surface loading, that is,

$$\Gamma_{metal}\ (\mu mol/m^2) = \frac{(C_{metal,initial} - C_{metal,final})\ (\mu mol/L)}{SL\ (m^2/L)}.$$

2.4. Catalyst preparation and characterization

Catalyst synthesis by strong electrostatic adsorption and dry impregnation has bee described previously [7]. In brief, via SEA, metals are adsorbed onto the support from an excess of solution at the pH of strongest interaction, as determined from the uptake–pH survey, and the same weight loading of metal is pore-filled into the support in DI. The TPR, STEM, and EDXS preparation and characterization methods have been described previously [7].

3. Results

The pH shifts of the three SBA-15 materials without metal in the solution at a surface loading of 1000 m^2/L are shown in Fig. 1a. The SBA-15 materials have virtually the same pH shift profile as the amorphous silica (Vn-3s). From this profile, it can be seen that both amorphous silica and mesoporous silica have similar PZC values, around 4. Fig. 1b displays the pH shifts without metal in solution of SBA-15-3 and amorphous silica at 10,000 m^2/L. At this higher loading, the pH plateaus are more evident, and the width of the Vn-3S material appears to be slightly greater than that of SBA-15. Model fits are shown as the solid and dashed lines; we discuss these later.

Fig. 2 displays the SBA-15 dissolution as a function of pH without metal in solution at a contact time of 1 h. All of the curves indicate an increase in silica dissolution with increasing pH in the basic region. The dissolution of mesoporous silicas in the high pH range after 1 h is significantly greater that of the amorphous silica for all samples except SBA-15-3 at a final pH of 13. A 1-h contact with sodium hydroxide solution equilibrated at pH 10 causes a slight decrease in the surface area, from 578 to 531 m^2/g for SBA-15-2 (Table 2), but large increases in the pore volume (from 0.566 to 0.718 cm^3/g) and mean pore diameter (from 40.3 to 54 Å). After metal adsorption, the surface area of a 9.15 wt% Pt SBA-15-2 sample dropped to 365 m^2/g after drying at room temperature, was slightly higher at 391 m^2/g after drying at 100 °C, and returned to 493 m^2/g after reduction at 160 °C, which is about 7% below the value for the 1-h NaOH-contacted sample (531 m^2/g).

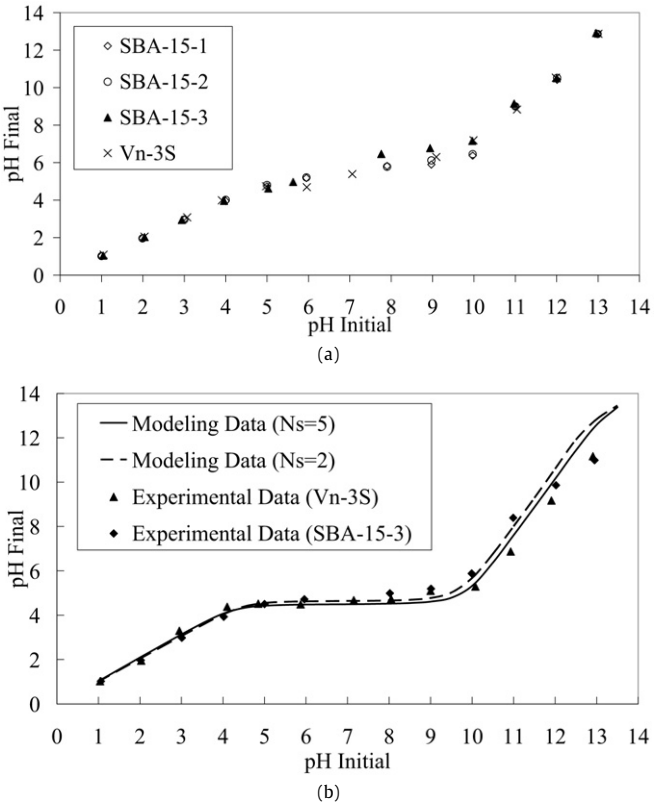

Fig. 1. Control experiments in metal-free solutions: (a) pH shift data for metal-free solutions contacted with SBA-15 and Vn-3S at 1000 m^2/L; (b) pH shift experimental data and modeling data for metal-free solutions contacted with SBA-15 and Vn-3S at 10,000 m^2/L (model fit obtained using PZC = 4.2, ΔpK = 7.0).

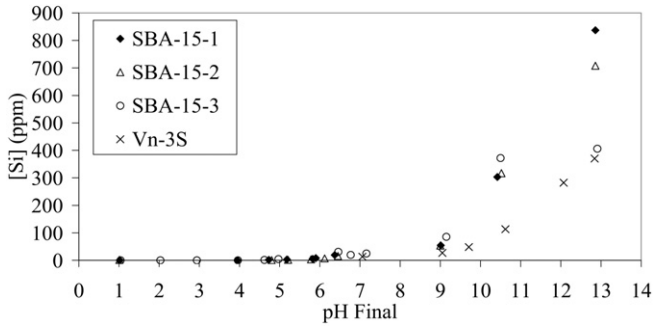

Fig. 2. SBA-15 dissolution versus pH at 1000 m^2/L in metal-free (control) solutions.

Figs. 3a–3c display uptake versus pH curves at constant metal concentration over SBA-15-3, SBA-15-1, and SBA-15-2. Fig. 3a contains the data for $[Pd(NH_3)_4]^{+2}$, $[Cu(NH_3)_4]^{+2}$, $[Co(NH_3)_6]^{+3}$, $[Ru(NH_3)_6]^{+3}$, and $[Ru(NH_3)_6]^{+2}$ over SBA-15-3. No adsorption occurs when the final pH is below the PZC of SBA-15-3 (~4.0). The SBA-15 begins to adsorb metal ammine complexes at a pH greater than pH_{PZC} and reaches a maximum uptake in the pH range of 10-11. Beyond a pH of 11, a decrease in adsorption is observed. Compared with the amorphous silica, the pH of maximum uptake for SBA-15 is a bit lower. Figs. 3b and 3c show the adsorption of the noble metal ammine complexes $[Pt(NH_3)_4]^{+2}$ and base metal ammine complexes $[Co(NH_3)_6]^{+3}$ over SBA-15-1 and SBA-15-2. For 1-h contact, the adsorption of $[Co(NH_3)_6]^{+3}$ does not decrease at high pH values of 12–13, whereas for 24-h contact, it reaches a much higher maximum uptake around a final pH of 11 and then decreases to 0 when the pH approaches 13. This is due to the extensive dissolution of the silica at the long contact time. On the

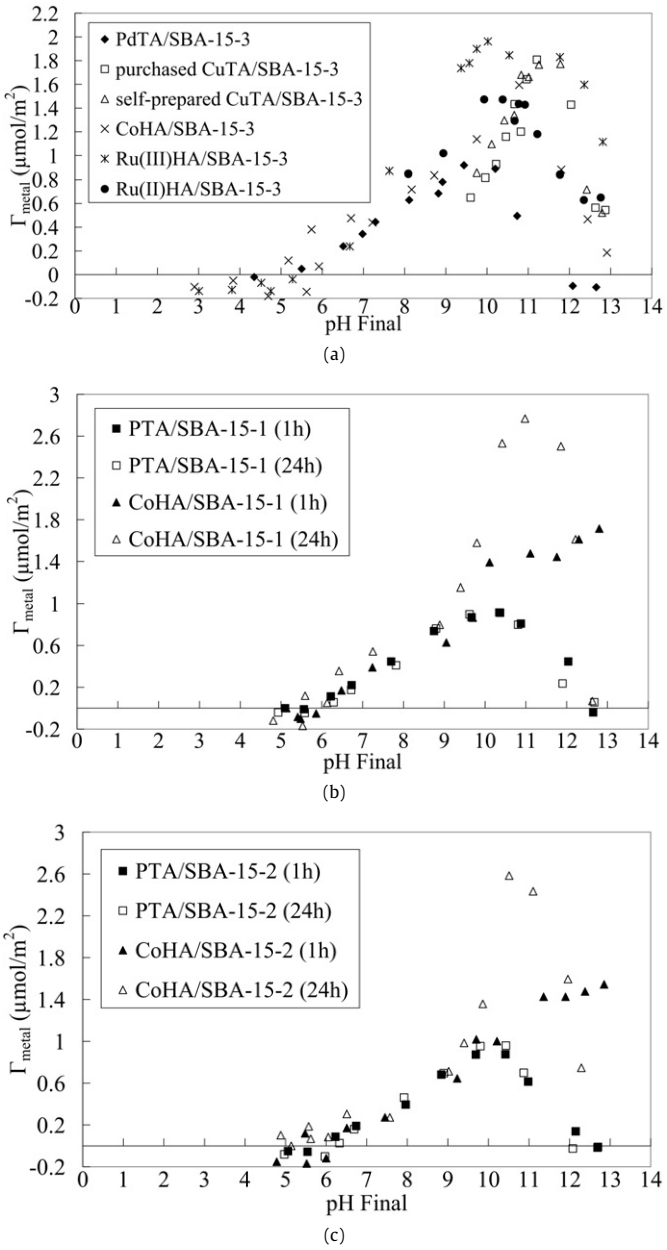

Fig. 3. Metal surface density vs. various pHs at surface loading 1000 m^2/L: (a) Pd, Cu, Co, Ru ammine complexes over SBA-15-3 (contact time = 1 h), (b) PTA and CoHA over SBA-15-1 (contact time = 1 and 24 h), (c) PTA and CoHA over SBA-15-2 (contact time = 1 and 24 h).

other hand, the 1-h and 24-h adsorption profiles of $[Pt(NH_3)_4]^{+2}$ at various pH values over SBA-15-1 and SBA-15-2 almost overlap.

Adsorption kinetics are shown in Fig. 4, which contains plots of pH_{final} versus time (a) and Pt surface density versus time (b). The initial pH for the kinetics experiments was chosen from the pH shift control experiment of Fig. 1a so as to yield the optimal pH for each material (11.5 [7] and 10 [Fig. 3] for amorphous and mesoporous silica, respectively). The adsorption equilibrium, which corresponds to 9.2 wt% Pt, is attained within 5 min for the mesoporous silica and within 10 min (3.0% Pt) for the microporous amorphous silica, even though the pH is not fully equilibrated over either substrate.

The TPR patterns of dried unreduced catalyst samples are summarized in Fig. 5. The Pt-containing samples based on SBA-15-1 and SBA-15-2 display similar reduction profiles. The PdTA/SBA-15-3 profile (Fig. 5c) is quite similar to the PdTA/Vn-3S TPR profile re-

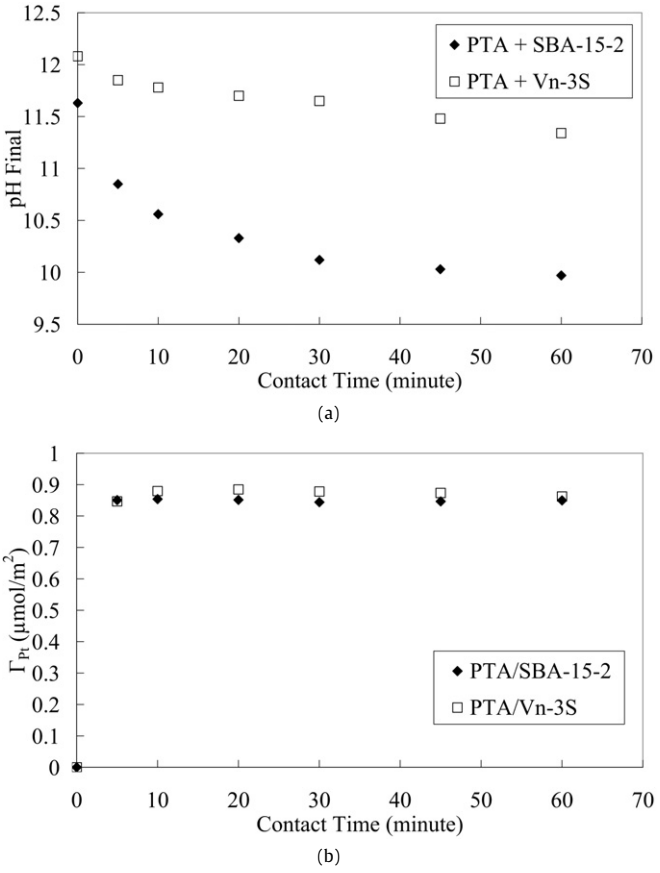

Fig. 4. Adsorption kinetics measurement of PTA on SBA-15-2 and Vn-3S at optimal pH for maximum uptake: (a) pH change at various contact time, (b) uptake of $[Pt(NH_3)_4]^{+2}$ at various contact time.

ported in Part I of this work [7]. The TPR profiles of Co(III)HA/SBA-15-1 and Co(III)HA/SBA-15-2 (Figs. 5d and 5e) have only one main peak and are similar to the TPR profile of Co(III)HA/Vn-3S in Part I [7].

In all cases, the reduction peaks of the SEA-prepared metals shift to higher temperatures and are broader relative to the DI-prepared metal, as with the TPR patterns of metals on amorphous silica (Fig. 7 in Part I [7]). The stronger interaction between adsorbed species and silica resulting from the SEA preparation makes the metal precursor much more difficult to reduce. The reduction of SBA-15-supported cobalt ammine (Figs. 5d and 5e) is lower by about 100 °C than that of amorphous silica-supported Co (Fig. 7c in Part I [7]), whereas the SBA-15-supported Pd peak (Fig. 5c) may be slightly lower that the corresponding amorphous silica-supported sample (Fig. 7a in Part I [7]). The peak shapes of the SBA-15-supported Pd and Co have a relatively narrower aspect than those of the amorphous silica-supported metals, which are shorter and wider. The narrower width of the mesoporous silica-supported metals likely arises from the narrow pore size distribution of these materials. The wider pore size distribution of the amorphous silica could lead to a wider range of precursor–support interactions during reduction.

High-angle annular dark-field (Z-contrast) images were obtained for each sample prepared via SEA and DI at the various metal loadings shown in Table 3 and used to obtain the particle size distributions and standard deviations. These particles were prepared using only a reduction step, determined from the TPR profiles of Fig. 5, with no intermediate calcination as has been used in previous studies of electrostatic adsorption over MCM-41 [25–27] or SBA-15 [17] materials. A comprehensive set of represen-

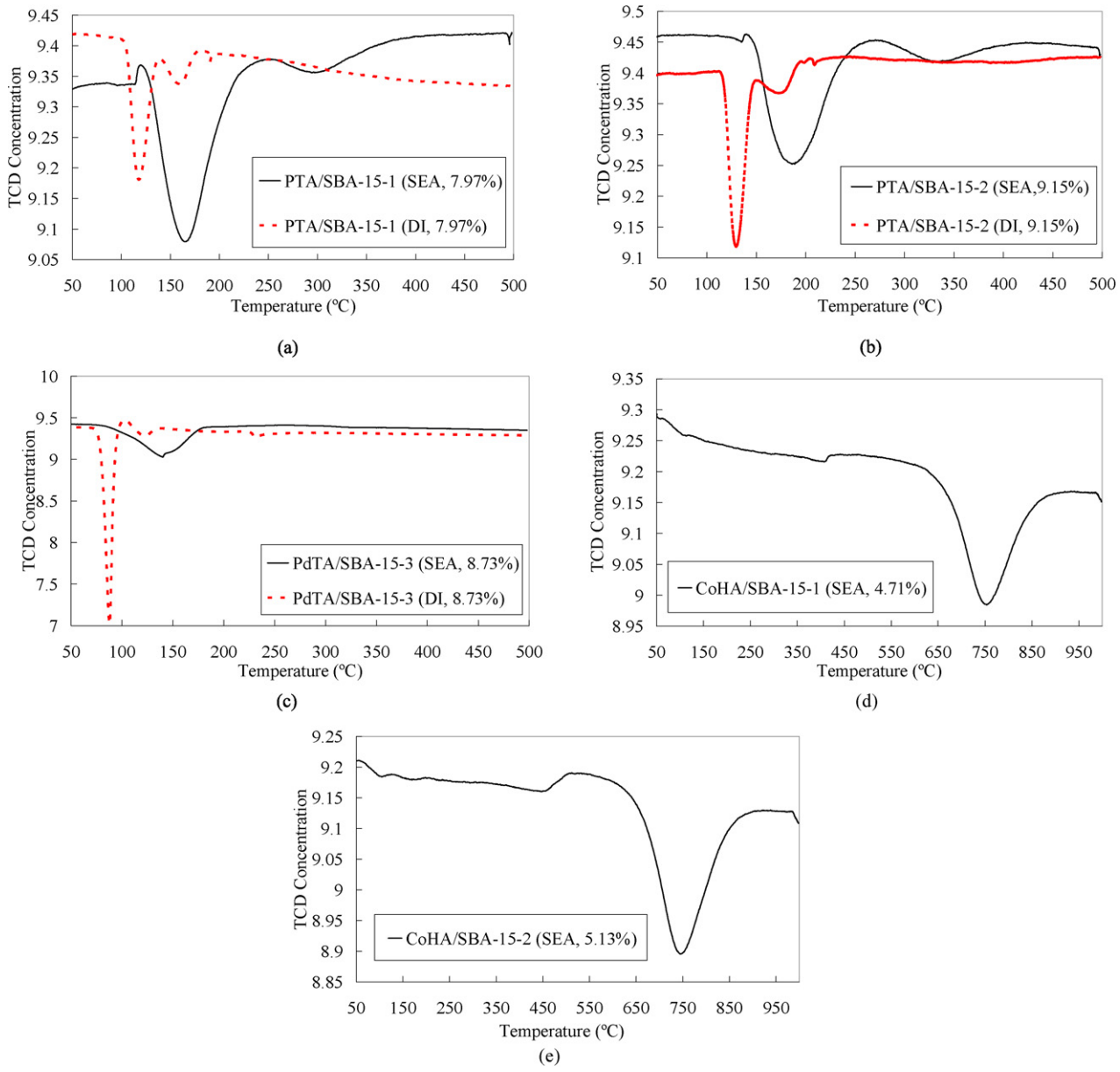

Fig. 5. TPR patterns of dried unreduced samples: (a) PTA/SBA-15-1, (b) PTA/SBA-15-2, (c) PdTA/SBA-15-3, (d) CoHA/SBA-15-1, (e) CoHA/SBA-15-2.

tative Z-contrast images and particle size distributions is given in the supplementary material, Figs. S1–S7.

Selected STEM images of Pt are shown in Fig. 6. For the Pt/SBA-15-1 sample (Fig. 6a), the SEA method yields small metal particles, which appear to form homogeneously throughout the pore volume of the SBA-15. Tilting experiments in which images of the same region of sample were obtained at ±20 degrees revealed that particles in the center of the SBA-15 bundles did not move as the sample was tilted, but the particles at the edge did move; this further confirms the homogeneous distribution of metal in the pores. The larger particles within the size distribution (still narrow; Table 3) appeared to be on the outer surface of the material. With a 350 °C reduction, an average particle size of 21 Å was achieved at 8.0 wt% for the SBA-15-1 sample (Fig. 6a) and an average particle size of 24 Å was achieved at 9.2 wt% for the SBA-15-2 sample (Fig. S2a and Table 3). The respective particle sizes were decreased to 19 and 18 Å with a 160 °C reduction (Fig. 6b and Fig. S7a). Results for the short-contact (5 min) impregnation are shown in Fig. 6c; the average Pt particle size of Pt/SBA-15-2 after 5 min of contact was 25 Å, very close to that of the sample prepared after 1 h of contact (24 Å; Fig. 6a). The average particle size of Pt/Vn-3S prepared with 5 min of contact was 13 Å (Fig. S7b), which is also close to the value of 10 Å reported previously with Pt/Vn-3S [30]. Finally, the DI method tended to generate large rod-like metal clusters along channels and on the exterior surfaces (Fig. 6d).

The STEM images of Pd on SBA-15-3 (Fig. 7a) demonstrate the similar trend that SEA generates small and homogeneous particles, whereas the DI method results in large and poorly dispersed particles after reduction (Fig. 7b). A 200 °C reduction could be used for Pd; this resulted in an average particle size of 13 Å for the SEA preparation at 8.7 wt% using SBA-15-3.

Fig. 7c shows that the high reduction temperature needed for the Co samples (800 °C) had a deleterious effect on particle size and particle distribution, although the sizes for SEA prepared samples are much smaller than those for the DI samples reduced at much lower temperature (450 °C) shown in Fig. 7d. Sizes ranged from 73 to 95 Å for 2.4–5.1 wt% Co supported on SBA-15-1 and SBA-15-2 for the SEA preparations. Significant migration was evident within and to the exterior of the SBA-15 particles.

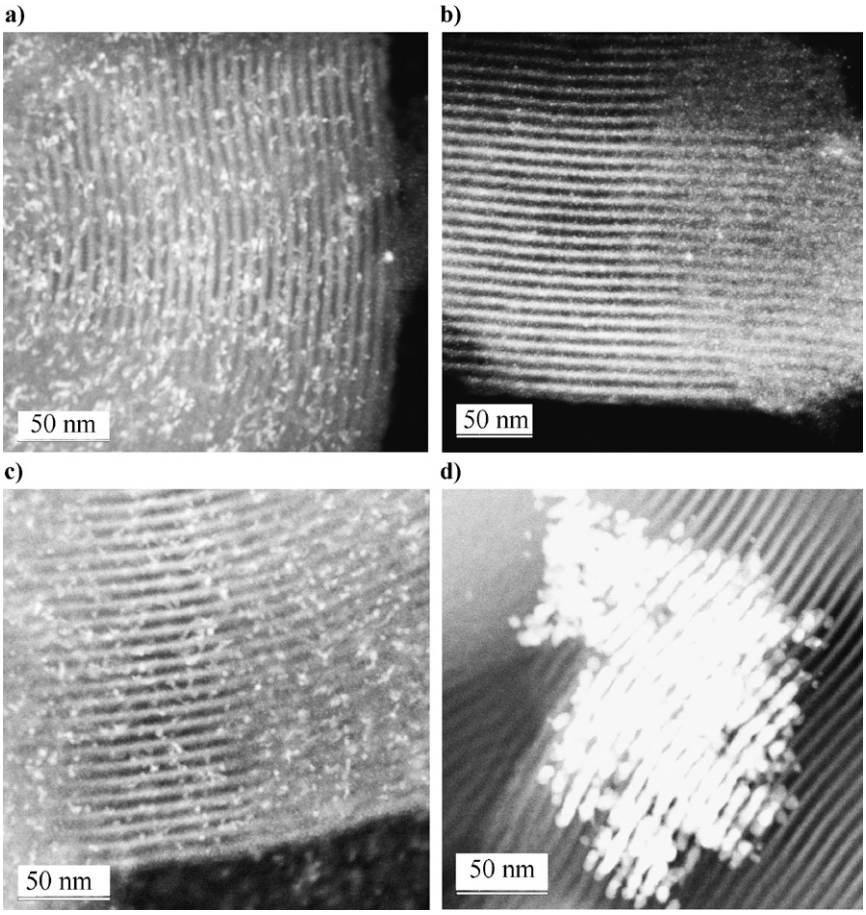

Fig. 6. Representative STEM images of reduced Pt particles: (a) 8.0 wt% Pt/SBA-15-1 (SEA, 1-h contact, reduced at 350 °C), (b) 8.0 wt% Pt/SBA-15-1 (SEA, 1-h contact, reduced at 160 °C), (c) 9.2 wt% Pt/SBA-15-2 (SEA, 5-min contact, reduced at 350 °C), and (d) 8.0 wt% Pt/SBA-15-1 DI sample (1-h contact, reduced at 350 °C).

4. Discussion

4.1. Mechanistic comparison with amorphous silica

A small difference in the pH plateau width for amorphous silica and SBA-15 can be seen in Fig. 1b. This difference can be crudely simulated using a value for the hydroxyl group density (N_S) of 2 OH/nm^2 for the mesoporous material versus the normal value of 5 OH/nm^2 [31] for amorphous silica. These results suggest that mesoporous silica SBA-15 has a lower hydroxyl group density than amorphous silica. A study of OH density over SBA-15 with pyridine ^{15}N MAS NMR yielded an estimated value of 3.7 OH/nm^2 [32]. Even at 2 OH/nm^2, there would appear to be a sufficient density of OH groups to strongly adsorb the metal ammine complexes via an electrostatic mechanism, because the maximum adsorption densities shown in Fig. 3 (especially for the most robust Pt and Pd ammine complexes) are very similar to those over amorphous silica [7,30]. Surface density limits of electrostatic adsorption are steric and are determined by the size of the adsorbing complex plus its number of hydration sheaths, which is typically 1 for anions and 1–2 for cations [8]. Maximum electrostatic uptake of typical metal ammine complexes of 1–2 μmol/m^2, corresponding to two or one hydration sheath(s), equates to about 0.5–1 complex per nm^2 [8]; the higher figure would be electrically saturated by a surface with 2 OH/nm^2. Electrostatic adsorption has not been considered a function of OH density given the large size of hydrated coordination complexes compared with typical ranges of OH densities [31]. Experiments comparing alpha alumina with low surface OH density and gamma alumina with high OH density also have borne this out [33].

In a deposition–precipitation study using Pt tetraammine [12], electrostatic interactions were cited, although the precipitating species was postulated to be Pt hydroxide. The final pH of the process was only slightly above 6, however, and if electrostatic adsorption were to occur, it would not be very weak, as indicated by the uptake–pH plots of Fig. 3. Uptake only just began at pH 6. Weak electrostatic interactions may explain the poor dispersion of the tetraammine complex prepared via DP relative to the chloroplatinic acid complex prepared via IWI [12].

Previous work also has suggested that an electrostatic mechanism can prevail even while support dissolution is considerable; as metal atoms dissolve from the surface, additional OH groups can form [34]. The lower surface areas and pore volumes of the impregnated and dried samples (Table 2) reflect the filling of pores by at least partially hydrated ammine complexes. As the drying becomes more rigorous, the surface area and pore volume increase; reduction appears to remove all material but the metal, because the surface area and pore volume of the 9.15 wt% Pt sample (493 m^2/g and 0.67 cm^3/g) are in reasonable agreement with those of the 1-h NaOH-contacted, metal-free SBA-15 substrate (531 m^2/g and 0.72 cm^3/g).

Generally speaking, the adsorption behavior of metal ammines over SBA-15 looks similar to that over amorphous silica [7]. When the pH is less than the PZC of SBA-15, no adsorption occurs. Adsorption occurs only when the final pH is higher than the PZC, and a maximum uptake occurs around a final pH of 10–11. Adsorption is retarded in a highly basic solution, with the exception of cobalt over the SBA-15-1 and -2 samples. The adsorption mechanism of metal ammines over SBA-15 can be attributed largely to

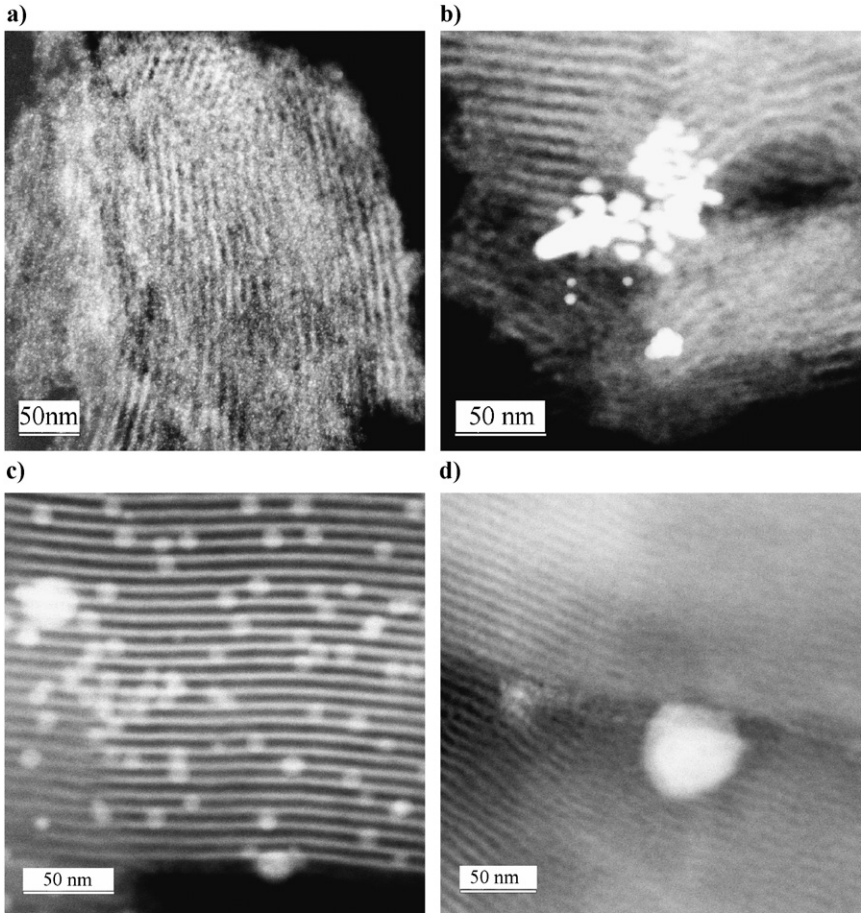

Fig. 7. Representative STEM images of reduced Pd and Co particles: (a) 8.7 wt% Pd/SBA-15-3 (SEA), (b) 8.7 wt% Pd/SBA-15-3 (DI), (c) 4.7 wt% Co/SBA-15-1 (SEA), and (d) 4.7 wt% Co/SBA-15-1 (SEA).

electrostatic interaction, with some variation for the reactivity of less-stable base metal ammine complexes, as noted previously [7].

The reactivity of cobalt ammines is most evident in Figs. 3b and 3c at the 1-h contact time, when no retardation of Co uptake at high pH occurs. The continued high uptake of cobalt can be attributed to the formation of cobalt phyllosilicates of the $CoO(OH)(Si_2O_5)_2$ or $Co(OH)_2(Si_2O_5)_2$ type [35,36]. These cobalt phyllosilicates would precipitate on the SBA-15 surface, thus increasing the surface density. This occurs to a lesser degree over the SBA-15-3 material (Fig. 3a), which is less soluble at the higher pH (Fig. 1b). At pH 12–13 at 24 h of contact (Figs. 3b and 3c), it appears that the SBA-15-1 and SBA-15-2 dissolve almost completely, causing any adsorbed species to return into solution. The PTA and PdTA complexes are much more stable than CoHA and do not exhibit this behavior.

For the copper tetraammine complex, maximum adsorption is not as high over SBA-15 as over amorphous silica Vn-3S [7]. Over the amorphous support, Cu uptake occurs at a maximum surface density of about 2.5–2.6 μmol/m^2, whereas (from Fig. 3a) the maximum uptake of 1.8-1.9 μmol/m^2 was observed for self-prepared and purchased CuTA. In previous papers [7,37], the excess adsorption of Cu over Vn-3S was attributed to the formation of the copper dimer $Cu_2(OH)_2^{2+}$, which occurs in response to the decreased local pH at the adsorption plane. Comparing the two supports, we see that the optimal pH for maximum uptake is 10–10.5 over SBA-15 (Fig. 3a) and 11–11.5 over Vn-3S [7]. Starting from a lower bulk pH, the local pH in the SBA-15 mesopores conceivably can become too low to promote copper dimer formation.

4.2. Practical considerations

The level of surface density attained as well as STEM imaging suggest that the entire internal surface of the SBA-15 materials has adsorbed metal ammines, leading to a homogeneous deposition of metals in the pore structure of SBA-15. Mild reductions, such as can be used with Pt and Pd, can yield ultra-small metal particles even at high loadings. Particle sizes for these two metals are on the order of 2.0 and 1.3 nm, respectively, at loadings of up to 9 wt%. These loadings are about an order of magnitude higher than those cited in Table 1, and the particle sizes are among the smallest reported. In addition, standard deviations of the particle size distributions are typically 25% of the particle size (Table 2). The 1.3-nm average size of the 4.6 and 8.7 wt% Pd materials is considerably smaller than the 3.6-nm particles reported for ion-exchanged Pd [17] using the same precursor. In that study, however, calcination at 550 °C was used, which could have sintered the metal phase.

The SEA method is much less complicated that the urea deposition–precipitation method used with Pt tetraammine over SBA-15 in a previous study [12]. That method yielded 3.4-nm Pt particles at 0.5 wt%, with larger (15-nm) particles on the exterior of the SBA-15. With SEA, 1.8-nm particles are achieved at 9.2 wt% quite homogeneously throughout the internal pore volume of the SBA-15. The impregnation step consists of contacting the SBA-15 support with the correctly basified solution for 5 min, followed by filtering, drying, and reducing.

When high reduction temperatures are needed (as in the case of cobalt), the metal particles do appear to sinter considerably on reduction and can migrate to the exterior surfaces of the substrate. (Even with the high reduction temperature, the SEA-produced Co

Table 3
Average particle size and size distribution (σ) of the reduced catalysts prepared by SEA and DI: (a) Pt/SBA-15-1 and Pt/SBA-15-2, (b) Pd/SBA-15-3, (c) Co/SBA-15-1 and SBA-15-2.

Catalyst	Precursor	Pt %	Preparation method	Reduction temperature (°C)	Average diameter (Å)	σ (Å)
			(a) Pt			
Pt/SBA-15-1	PTA	8.0	SEA	350	21	6.6
Pt/SBA-15-1	PTA	4.2	SEA	350	36	10
Pt/SBA-15-2	PTA	9.2	SEA	350	24	6.7
Pt/SBA-15-2	PTA	5.0	SEA	350	20	9.7
Pt/SBA-15-1	PTA	8.0	SEA	160	19	5.3
Pt/SBA-15-1	PTA	4.2	SEA	160	20	5.0
Pt/SBA-15-2	PTA	9.2	SEA	160	18	4.5
Pt/SBA-15-2	PTA	5.0	SEA	160	18	5.1
Pt/SBA-15-1	PTA	8.0	DI	350	87	27
Pt/SBA-15-1	PTA	4.2	DI	350	91	29
Pt/SBA-15-2	PTA	9.2	DI	350	130	62
Pt/SBA-15-2	PTA	5.0	DI	350	100	38
			(b) Pd			
Pd/SBA-15-3	PdTA	8.7	SEA	200	13	4.3
Pd/SBA-15-3	PdTA	4.6	SEA	200	13	3.2
Pd/SBA-15-3	PdTA	8.7	DI	200	110	52
Pd/SBA-15-3	PdTA	4.6	DI	200	110	53
			(c) Co			
Co/SBA-15-1	CoHA	4.7	SEA	800	95	55
Co/SBA-15-1	CoHA	2.4	SEA	800	82	42
Co/SBA-15-2	CoHA	5.1	SEA	800	73	28
Co/SBA-15-2	CoHA	2.6	SEA	800	77	26
Co/SBA-15-1	CoHA	4.7	DI	450	250	110
Co/SBA-15-1	CoHA	2.4	DI	450	360	110
Co/SBA-15-2	CoHA	5.1	DI	450	450	350
Co/SBA-15-2	CoHA	2.6	DI	450	130	110

particles are much smaller than DI samples.) Because the cobalt ammine precursor appears to be very stable when adsorbed onto silica [38], alternate procedures might be used to lower the reduction temperature. Cobalt [36] and nickel [39] ethylenediammine complexes have been used as precursors, and these appear to have a lower decomposition temperature compared with the ammines. Controlled thermal decomposition using DI with nitrate salts recently has been shown to be effective at synthesizing moderately small Ni particles at high Ni loading [40].

The dissolution data shown in Fig. 2 and the surface area data given in Table 2 suggest that the dissolution of SBA-15 at the optimal final pH (about 10) is significant. Interpolating Fig. 2, a dissolved Si level of about 250 ppm at pH 10 represents about 25% of the mass of the silica. The large change in pore volume from 40 to 54 Å is consistent with the removal of a significant fraction of mass. STEM characterization, on the other hand, indicates that the structure of the SBA-15 remains relatively intact with a 1-h contact time. For MCM-41 materials, instability of the structure limits the impregnation to a pH value of 7.5 [27] or 8 [25,26]; otherwise, the structure is severely compromised. Although dissolution is still significant, the thicker walls of SBA-15 allow it to be used at the higher final pH, where more metal can be adsorbed. If less metal loading is desired, of course, a lower final pH can be used.

Otherwise, to minimize silica dissolution, a 5-min impregnation can be used (Fig. 4), during which all metal adsorbs and ultra-small metal particles are formed (Fig. 6c). Another method for minimizing dissolution would be to approach the final pH of 10 only after the silica has equilibrated with a neutral solution (i.e., from low pH to high), instead of with the initial pH of 11.5 (see Fig. 4) used to overcome the pH-buffering step. The added complexity of sequential pH control to minimize dissolution may prove worthwhile should dissolved Si pose a problem for a particular catalytic reaction.

For the low-temperature-reducing metals at least, these results demonstrate that the SEA method can be readily applied to mesoporous silica materials to yield small particles with a tight size distribution. The weight loading versus surface area plot (Fig. 10 of Part I [7]), which establishes the weight loading limits of a single-step SEA synthesis, can be applied to both mesoporous and microporous silica. For example, because PTA adsorbs at about 0.86 over silica (all silicas, amorphous and mesoporous), for a 1000-m^2/g SBA-15-3 material, it should be possible to adsorb 0.86 μmol Pt/m^2 × 1000 m^2/g silica × 195 × 10^{-6} g Pt/μmol Pt = 0.17 g Pt/g silica, or over 14 wt% Pt in a single step, and at that loading obtain <2-nm particles with a 160 °C reduction. A mesoporous silica-supported 15% Pt catalyst synthesized by IWI with chloroplatinic acid [9] reported a particle size >10 nm, and another for 8 wt% Pt also prepared from chloroplatinic acid reported 20-nm particles [14]. This calculation holds true for the other metals, including base metals, which often are used at higher loadings.

5. Conclusion

In previous work, it was shown that PTA adsorbed via an electrostatic mechanism over various precipitated and fumed silicas with widely varying surface areas [31], and that this method was superior to dry impregnation for synthesizing highly dispersed particles [30]. In this set of papers, the SEA method has been extended to other metal ammine complexes over amorphous silica (Part I [7]) and over mesoporous silica (Part II). The SEA method appears to be a rational procedure for the cheap, simple, and scalable preparation of highly dispersed supported catalysts for all ammine complexes and all types of silica.

Acknowledgments

This work was supported by the National Science Foundation (grant CTS-0208181). The authors thank Jelle R.A. Sietsma, Utrecht University and Dr. Jianfeng Yao, Monash University for providing the SBA-15 materials.

Supplementary material

The online version of this article contains additional supplementary material.

Please visit DOI: 10.1016/j.jcat.2008.09.023.

References

[1] C.T. Kresge, M.E. Leonowicz, W.J. Roth, J.C. Vartuli, J.S. Beck, Nature 359 (1992) 710.
[2] D.Y. Zhao, J.L. Feng, Q.S. Huo, N. Melosh, G.H. Fredrickson, B.F. Chmelka, G.D. Stucky, Science 279 (1998) 548.
[3] J.Y. Ying, C.P. Mehnert, M.S. Wong, Angew. Chem. Int. Ed. 38 (1999) 56.
[4] K.W. Gallis, J.T. Araujo, K.J. Duff, J.G. Moore, C.C. Landry, Adv. Mater. 11 (1999) 1452.
[5] A.L. Doadrio, E.M.B. Sousa, J.C. Doadrio, J.P. Pariente, I. Izquierdo-Barba, M. Vallet-Regi, J. Controlled Release 97 (2004) 125.
[6] C. Yang, P.-H. Liu, Y.-F. Ho, C.-Y. Chiu, K.-J. Chao, Chem. Mater. 15 (2003) 275.
[7] L. Jiao, J.R. Regalbuto, J. Catal. (2008), doi:10.1016/j.jcat.2008.09.022.
[8] J.R. Regalbuto, in: J.R. Regalbuto (Ed.), Catalyst Preparation: Science and Engineering, Taylor and Francis/CRC Press, Boca Raton, FL, 2007, p. 161.
[9] L.-X. Zhang, J.-L. Shi, J. Yu, Z.-L. Hua, X.-G. Zhao, M.-L. Ruan, Adv. Mater. 14 (2002) 1510.
[10] K.S. Oh, S.I. Woo, Catal. Lett. 110 (2006) 247.
[11] E. Molnar, Catal. Lett. 101 (2005) 159.
[12] S. Chytil, W.R. Glomm, I. Kvande, T. Zhao, E.A. Blekkan, Micropor. Mesopor. Mater. 86 (2005) 198.
[13] S. Chytil, W.R. Glomm, I. Kvande, T. Zhao, J.C. Walmsley, E.A. Blekkan, Top. Catal. 45 (2007) 93.
[14] C.-M. Yang, P.-H. Liu, Y.-F. Ho, C.-Y. Chiu, K.-J. Chao, Chem. Mater. 15 (2003) 275.

[15] R.M. Rioux, J. Phys. Chem. B 109 (2005) 2192.
[16] J. Arbiol, A. Cabot, J.R. Morante, Appl. Phys. Lett. 81 (2000) 3449.
[17] I. Yuranov, P. Moeckli, E. Suvorova, P. Buffat, L. Kiwi-Minsker, A. Renken, J. Mol. Catal. A 192 (2003) 239.
[18] I. Yuranov, L. Kiwi-Minsker, A. Renken, Appl. Catal. B 43 (2003) 217.
[19] C.-H. Tu, A.-Q. Wang, M.-Y. Zheng, X.-D. Wang, T. Zhang, Appl. Catal. A 297 (2006) 40.
[20] A. Martínez, C. López, F. Márquez, I. Díaz, J. Catal. 220 (2003) 486.
[21] A.Y. Khodakov, A. Griboval-Constant, R. Bechara, V.L. Zholobenko, J. Catal. 206 (2002) 230.
[22] H. Li, J. Li, H. Ni, D. Song, Catal. Lett. 110 (2006) 71.
[23] J. Huang, T. Jiang, B. Han, W. Wu, Z. Liu, Z. Xie, J. Zhang, Catal. Lett. 103 (2005) 59.
[24] H. Li, R. Wang, Q. Hong, L. Chen, Z. Zhong, Y. Koltypin, J. Calderon-Moreno, A. Gedanken, Langmuir 20 (2004) 8352.
[25] B. Zhu, F. Letellier, J. Blanchard, K. Fajerwerg, C. Louis, D. Guillaume, D. Uzio, M. Breyesse, Stud. Surf. Sci. Catal. 162 (2006) 449.
[26] F. Letellier, J. Blanchard, K. Fajerwerg, C. Louis, M. Breyesse, D. Guillaume, D. Uzio, Catal. Lett. 110 (2006) 115.
[27] P. Tian, J. Blanchard, K. Fajerwerg, M. Breysse, M. Vrinat, Z. Liu, Micropor. Mesopor. Mater. 60 (2003) 197.
[28] D. Zhao, Q. Huo, J. Feng, B.F. Chmelka, G.D. Stucky, J. Am. Chem. Soc. 120 (1998) 6024.
[29] J. Park, J.R. Regalbuto, J. Colloid Interface Sci. 175 (1995) 239.
[30] J.T. Miller, A.J. Kropf, M. Schreier, J.R. Regalbuto, J. Catal. 225 (2004) 203.
[31] M. Schrier, J.R. Regalbuto, J. Catal. 225 (2004) 190.
[32] I.G. Shenderovich, G. Buntkowsky, A. Schreiber, E. Gedat, S. Sharif, J. Albrecht, N.S. Golubev, G.H. Findenegg, H.-H. Limbach, J. Phys. Chem. B 107 (2003) 11924.
[33] J.R. Regalbuto, S. Shadid, M. Bricker, D. Rende, J. Catal. 184 (1999) 335.
[34] N. Santhanam, T. Conforti, W. Spieker, J.R. Regalbuto, Catal. Today 21 (1994) 141.
[35] A. Loaiza-Gil, J. Arenas, M. Villarroel, F. Imbert, H. Del Castillo, B. Fontal, J. Mol. Catal. A 228 (2005) 339.
[36] R. Trujillano, F. Villain, C. Louis, J.-F. Lambert, J. Phys. Chem. C 111 (2007) 7152.
[37] M. Schreier, S. Terens, L. Belcher, J.R. Regalbuto, Nanotech. 16 (2005) S582.
[38] L. D'Souza, L. Jiao, J.T. Miller, A.J. Kropf, J.R. Regalbuto, J. Catal. 248 (2007) 165.
[39] S. Schimpf, C. Louis, P. Claus, Appl. Catal. A 318 (2007) 45.
[40] J.R.A. Sietsma, J.D. Meeldijk, J.P. Den Breejen, M. Versluijs-Helder, A.J. Van Dillen, P.E. de Jongh, K.P. de Jong, Angew. Chem. Int. Ed. 46 (2007) 4547.